ACS central science

http://pubs.acs.org/journal/acscii

Research Article

Parallel Automated Flow Synthesis of Covalent Protein Complexes That Can Inhibit MYC-Driven Transcription

Sebastian Pomplun,[▽] Muhammad Jbara,[▽] Carly K. Schissel, Susana Wilson Hawken, Ann Boija, Charles Li, Isaac Klein, and Bradley L. Pentelute*

Cite This: *ACS Cent. Sci.* 2021, 7, 1408−1418

Read Online

ACCESS | Metrics & More | Article Recommendations | Supporting Information

ABSTRACT: Dysregulation of the transcription factor MYC is involved in many human cancers. The dimeric transcription factor complexes of MYC/MAX and MAX/MAX activate or inhibit, respectively, gene transcription upon binding to the same enhancer box DNA. Targeting these complexes in cancer is a long-standing challenge. Inspired by the inhibitory activity of the MAX/MAX dimer, we engineered covalently linked, synthetic homo- and heterodimeric protein complexes to attenuate oncogenic MYC-driven transcription. We prepared the covalent protein complexes (~20 kDa, 167−231 residues) in a single shot via parallel automated flow synthesis in hours. The stabilized covalent dimers display DNA binding activity, are intrinsically cell-penetrant, and inhibit cancer cell proliferation in different cell lines. RNA sequencing and gene set enrichment analysis in A549 cancer cells confirmed that the synthetic dimers interfere with MYC-driven transcription. Our results demonstrate the potential of automated flow technology to rapidly deliver engineered synthetic protein complex mimetics that can serve as a starting point in developing inhibitors of MYC-driven cancer cell growth.

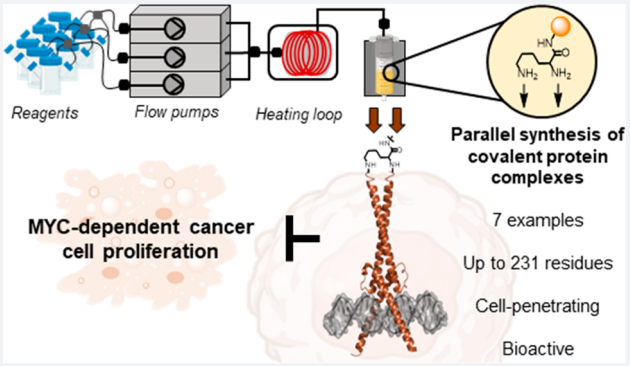

INTRODUCTION

Access to proteins is essential for academic and industrial research and for modern therapy development. Most proteins are obtained by biological expression. The chemical synthesis of proteins has emerged as a viable complementary approach and offers advantages, including the potential to incorporate unnatural amino acid or post-translational modifications. Chemical protein synthesis usually requires a combination of solid-phase and chemoselective ligation methods.[1−6]

The primary polypeptide sequences alone, however, are not sufficient for activity. Proteins fold into three-dimensionally defined secondary and tertiary structures to make possible diverse and complex tasks in living systems. Further, to reach their ultimate active architecture, many folded proteins form higher-order complexes containing multiple subunits.[7,8] Controlling the correct assembly of the desired subunits can be challenging and depends on complex stability, protein concentration, and protein localization. The identity and composition of the subunits forming a protein complex are crucial and determine the complex's activity.

The transcription factor protein MYC forms a heterodimer with MAX in order to bind to the E-Box DNA sequence (CACGTG).[9] The MYC/MAX protein complex is part of the basic-helix−loop-helix/leucine-zipper (bHLH/Lz) transcription factor family and initiates several cellular processes, including cell proliferation and survival.[10,11] MAX, alternatively, can homodimerize, compete for the E-Box DNA binding site, and inhibit MYC/MAX-driven transcription.[12] MYC/MAX and MAX/MAX, thus, have opposite activities, and MYC overexpression is observed in >50% of human cancers.[13−16]

Promising strategies to inhibit the oncogenic MYC activity rely on stabilizing the natural MAX/MAX dimer or delivering protein analogues with a similar mechanism of action. The targeting of MYC with small molecules has largely remained elusive, mainly because the structure of MYC presents no binding pockets for small molecule ligands.[17−22] To overcome the challenge of drugging MYC, Koehler et al. recently described a small molecule stabilizer of the MAX/MAX complex that inhibited the proliferation of several cancer cell lines and reduced the tumor burden in murine cancer models.[23] In a different approach, Soucek et al. developed the artificial miniprotein Omomyc: this dominant-negative form of MYC can compete for E-Box DNA binding and thus inhibit MYC/MAX-dependent transcription, ultimately result-

Received: June 1, 2021
Published: August 4, 2021

ing in tumor growth inhibition in various mouse models of cancer, causing only mild, well-tolerated, and reversible side effects.[24−27]

Omomyc, in the same way as the biological MYC and MAX proteins, has to form dimeric complexes to be functional and bioactive. MYC, MAX, and Omomyc can interact with each other in different combinations. Upon delivery of a monomer to the cell, the dominating complex formed depends on the other proteins' cellular concentrations and is hardly predictable.[25] The direct administration of defined and stable dimeric complexes would offer a superior degree of control over the concentration and composition of the bioactive dimer inhibitor, in addition to a potentially higher structural stability.

We reasoned that dimeric analogues of MYC and MAX, covalently linked in their bioactive form, could result in promising oncosuppressive modalities (Figure 1). Preparing

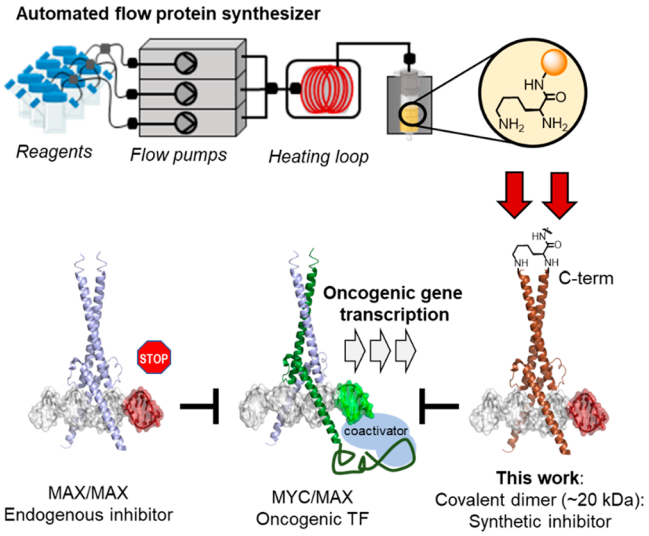

Figure 1. Covalent protein dimers prepared by automated flow protein synthesis (AFPS) are designed to compete with MYC/MAX for E-Box binding and inhibit oncogenic transcription. Inspired by the inhibitory activity of the MAX/MAX protein dimer assembly, we engineered covalently linked, synthetic homo- and heterodimeric analogues of MYC, MAX, and Omomyc, to inhibit MYC/MAX-dependent gene transcription.

homogeneous, stable, well-defined protein−protein conjugates can be a challenge.[28−30] Chemical synthesis approaches to generate covalently linked multimeric proteins have been mainly focused on preparing ubiquitinylated or sumoylated proteins.[31−38] These strategies relied on chemical ligation or chemoenzymatic workflows, requiring the incorporation of unnatural amino acids or an engineered recognition sequence, respectively. In addition, ligation-based strategies to prepare covalently linked HIV protease heterodimers have been reported by Torbeev et al., with the aim to study asymmetric mutations of this enzyme dimer.[39] Previous dimerization strategies of MYC/MAX analogues relied on disulfide formation at the C-terminus of the leucine zipper region of the transcription factor analogues.[40] Furthermore, in a pioneering study, Kent et al. chemically prepared MYC/MAX and MAX/MAX dimers connected via oxime linkages and thioesters.[41] While these defined dimers enabled DNA-binding studies, the reported strategies relied on dovetails with low chemical stability in a biological milieu, making them unsuitable for bioactivity studies in vivo.

We have previously shown that automated fast-flow protein synthesis (AFPS) enables direct access to defined, bioactive, and stable protein domains,[42,43] obviating the need for postsynthesis or expression dimerization reactions, such as native chemical ligation. Solid-phase flow chemistry has been used previously to generate branched glycans.[44] Here, we use AFPS for the parallel single-shot assembly of covalently linked MAX−MAX and Omomyc−Omomyc homodimers and MYC−MAX and Omomyc−MAX heterodimers. The covalent dimers (167−231 residues) were synthesized within hours, and after a single HPLC purification, these protein complexes were directly used for biological studies. Despite their considerable size, the protein dimers are intrinsically cell-penetrating and specifically inhibit MYC-dependent gene transcription and proliferation of cancer cells.

RESULTS

Single-Shot Flow Synthesis of Covalent Protein Dimers. We prepared covalent MAX−MAX **2** and Omomyc−Omomyc **3** homodimers by parallel single-shot fast-flow solid-phase synthesis. In MYC, MAX, and Omomyc dimers, the two C-termini of the DNA binding regions are in proximity to each other. SPPS proceeds from the peptide C-terminus to the N-terminus. Therefore, we envisioned obtaining the covalently linked protein dimers by assembling them starting from a bifunctional linker. We prepared linker **1** (Figure 2b) on a ChemMatrix Rink Amide resin (loading = 0.18 mmol/g). The linker contains an Alloc-protected lysine for late-stage modification, a β-alanine spacer, and a lysine with two free amine groups as a bifunctional starting point for the parallel synthesis. We loaded resin **1** into the fast-flow synthesizer reactor and prepared MAX−MAX **2** (164 residues, 3.4 h) and Omomyc−Omomyc **3** (184 residues, 3.7 h). As determined by in-line UV-Vis monitoring of the stepwise Fmoc deprotection, the synthesis of both dimers proceeded with high coupling efficiency at each coupling cycle (Figures S5 and S6). It is noteworthy that each step involved the parallel coupling and subsequent deprotection of two amino acids simultaneously. After cleavage and side-chain deprotection, LC-MS analysis indicated the desired products as the major component of both crude reaction mixtures. Upon preparative HPLC purification, we obtained pure MAX−MAX **2** and Omomyc−Omomyc **3** in 6% and 8% yield, respectively (Figure 2e,f). For advanced biological characterizations, we scaled up the Omomyc−Omomyc **3** preparation. For a single synthesis, we obtained 50 mg of pure material in 14% yield.

We synthesized covalent MYC−MAX **5** and Omomyc−MAX **6** heterodimers by consecutive single-shot fast-flow solid-phase synthesis. To enable the consecutive assembly of the heterodimers, we prepared resin **4** (Figure 2b): the bifunctional linker, in this case, is based on lysine protected with Alloc on its side-chain (Nε) amine. With the fast-flow synthesizer, we first assembled MAX from the α-amine of the lysine linker. For the last amino acid, we added Boc-glycine and removed the Alloc protection from the Nε of the lysine linker. On this amine, we then assembled MYC or Omomyc, respectively (Schemes S1 and S2). The synthesis time for each heterodimer amounted to ∼8 h (MYC−MAX **5**, 167 residues; Omomyc−MAX **6**, 175 residues). Both heterodimers were observed as the main component of the crude product mixture obtained from cleavage and side-chain deprotection. Upon preparative HPLC purification, we obtained pure MYC−MAX

https://doi.org/10.1021/acscentsci.1c00663
ACS Cent. Sci. 2021, 7, 1408−1418

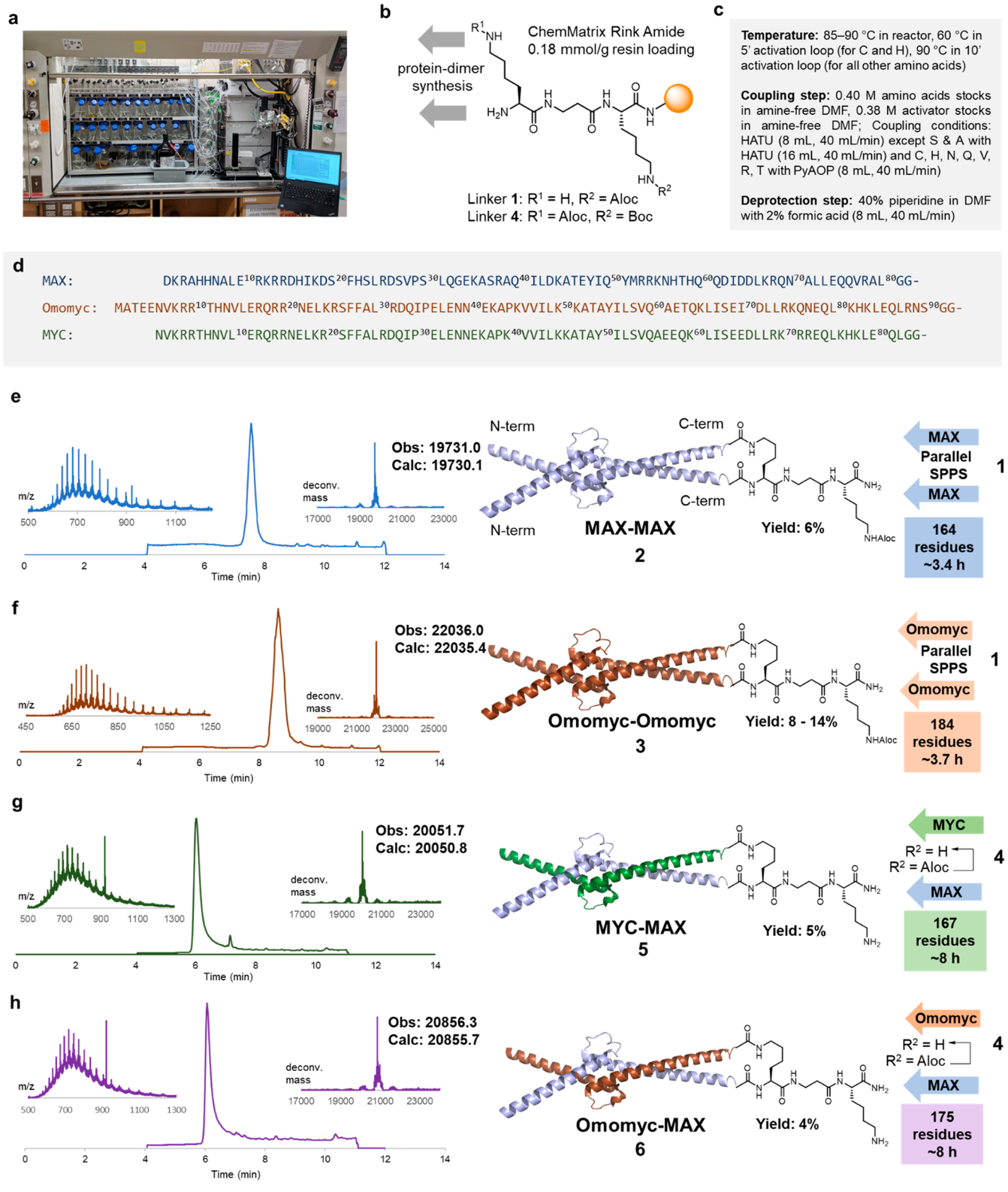

Figure 2. Covalently linked dimeric transcription factor analogues were prepared via fast-flow solid-phase synthesis. (a) An automated flow peptide synthesizer built in the Pentelute laboratory. (b) Resin for protein synthesis with lysine-based linkers **1** or **4** for parallel dimeric protein synthesis. The linkers were manually coupled on the Rink Amide resin prior to AFPS. (c) Reagents and conditions for flow synthesis. (d) Sequences of MYC, MAX, and Omomyc. (e–h) Synthesis time, yields, and LC-MS characterization of purified homodimers **2** and **3** and heterodimers **5** and **6**. The panels show the total ion current chromatogram (TIC) as the base spectrum, the electrospray ionization (ESI) mass-to-charge spectra (left inset), and deconvoluted mass spectra (right inset). The peak at 922 in the *m*/*z* spectra is the ion of the internal reference compound of the mass spectrometer. The minor MS peak population at masses lower than the expected product mass (in parts e, g, and h) is a mixture of deletion and truncation products.

https://doi.org/10.1021/acscentsci.1c00663
ACS Cent. Sci. 2021, 7, 1408–1418

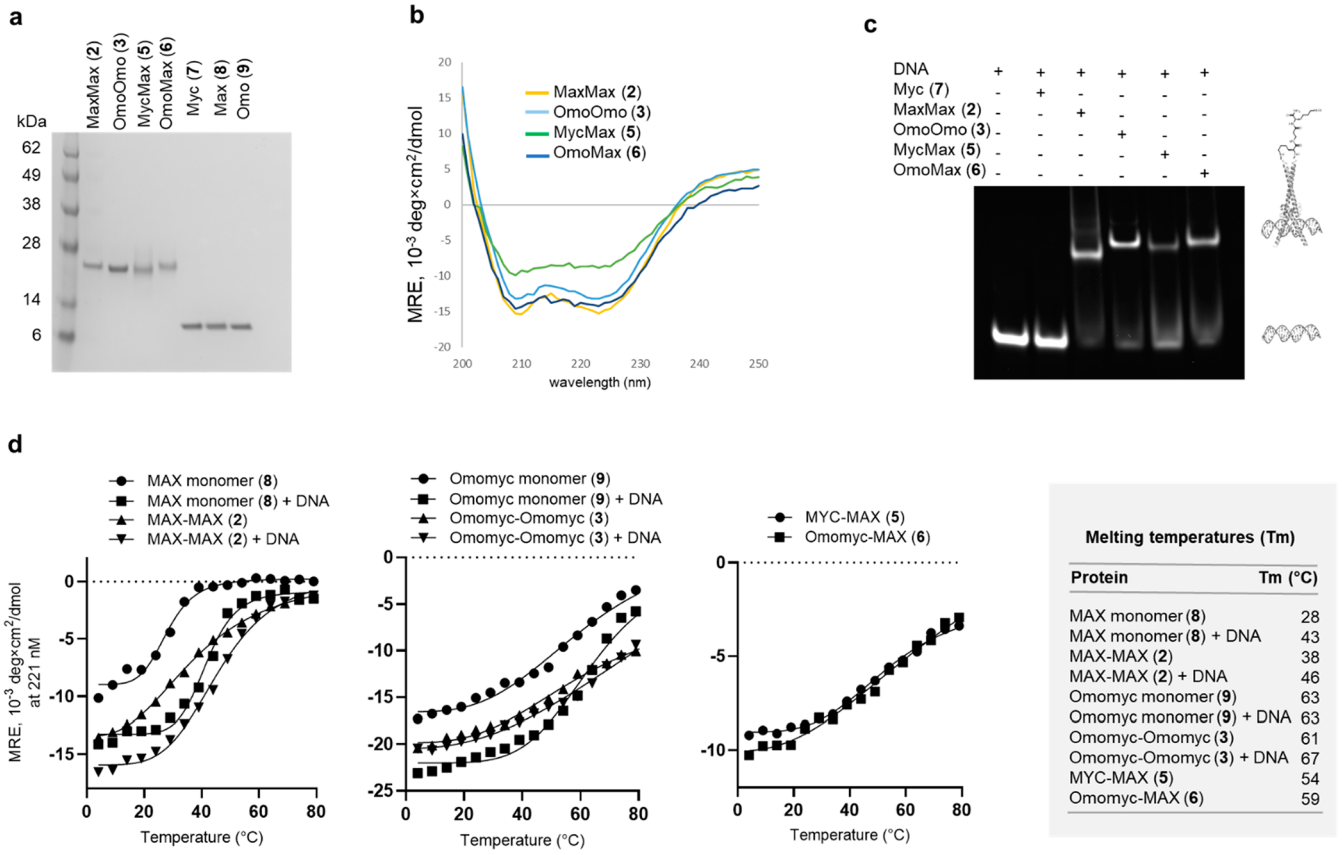

Melting temperatures (Tm)

Protein	Tm (°C)
MAX monomer (**8**)	28
MAX monomer (**8**) + DNA	43
MAX-MAX (**2**)	38
MAX-MAX (**2**) + DNA	46
Omomyc monomer (**9**)	63
Omomyc monomer (**9**) + DNA	63
Omomyc-Omomyc (**3**)	61
Omomyc-Omomyc (**3**) + DNA	67
MYC-MAX (**5**)	54
Omomyc-MAX (**6**)	59

Figure 3. The synthetic protein dimers are homogeneous, fold, and associate to E-box DNA. The covalent linkage stabilizes the structure and DNA/protein complexes. (a) SDS-PAGE analysis of synthetic protein dimers and monomers (∼1 μg per protein loaded). The bands were visualized by Coomassie Blue staining. (b) Proteins were dissolved in folding buffer (MES 10 mM, KCl 150 mM, $MgCl_2$ 1 mM, TCEP 1 mM, glycerol 10%, pH = 6.5) at 0.1 mg/mL, and full wavelength CD spectra were recorded from 250 to 200 nm at 4 °C. The *y*-axis shows the mean residual ellipticity (MRE) and the *x*-axis the wavelength. (c) Each compound was incubated with E-Box DNA in folding buffer (final concentrations: 2 μM protein and 1 μM DNA) for 1 h at room temperature. Samples were run on 10% polyacrylamide gel in TBE buffer and visualized with ethidium bromide. (d) For melting temperature determination, CD spectra were recorded at 221 nm from +4 to +89 °C, in 5 °C steps. (e) Summary table of melting temperatures determined by CD.

5 and Omomyc−MAX **6** dimers in 4% and 5% yield, respectively (Figure 2g,h).

Biophysical Characterization of the Synthetic Protein Dimers. Biophysical characterization confirmed the folding and DNA-binding activity of the four covalent protein dimers. We first analyzed dimers **2**, **3**, **5**, and **6** by sodium dodecyl sulfate polyacrylamide gel electrophoresis (SDS-PAGE). All dimer constructs had bands at the expected height of ∼20 kDa, and the monomers **7**−**9** (synthesized by AFPS, see the SI, sections 12.5−12.7) were observed at ∼10 kDa (Figure 3a). The refolding of the protein dimers did not require special procedures. We dissolved the lyophilized compounds in folding buffer (MES 10 mM, KCl 150 mM, $MgCl_2$ 1 mM, TCEP 1 mM, glycerol 10%, pH = 6.5), and all four dimers displayed defined α-helical signatures, as determined by circular dichroism (CD, Figure 3b). We next performed an electrophoretic mobility shift assay (EMSA) to determine the dimers' DNA binding activity. At a DNA concentration of 1 μM and protein concentration of 2 μM, all dimers formed complexes with the E-Box DNA, as observed by the shift retardation on the gel (Figure 3c). Monomeric MYC, tested as a negative control (4 μM), did not bind to E-Box DNA.

Covalently linked dimers have stabilized structures in aqueous buffer compared to their noncovalent analogues. We recorded CD signals at 221 nm between 4 and 89 °C (Figure 3d) to determine melting temperatures (T_m). With this method, we compared the noncovalent MAX/MAX (**8**/**8**) and Omomyc/Omomyc (**9**/**9**) dimers to our four synthetic covalent protein dimers (note: noncovalent dimers are indicated as protein/protein; covalent dimers are indicated as protein−protein). We also performed protein melting temperature measurements in the presence of equimolar E-Box DNA. Overall, the DNA stabilized the protein complexes' structures, in agreement with the literature.[26] The covalent linkage showed a significant stabilizing effect on the MAX dimers: we determined the T_m of the noncovalent MAX structure being 29 °C and the one of the covalent dimer 38 °C. Omomyc complexes, overall, displayed a higher structural stability than the other dimers tested. We did not observe a significant T_m difference for noncovalent Omomyc/Omomyc (**9**/**9**) compared to the covalent Omomyc−Omomyc (**3**). This observation might be explained by the greater stability of the Omomyc leucine zipper. The most stable complex of all structures tested was the covalent Omomyc−Omomyc dimer (**3**) in the presence of DNA, with a T_m of 67 °C. Finally, we tested the proteolytic stability of dimer **3**. After 1 h of incubation in human serum (5% in PBS) at 37 °C, we found 91% intact protein dimer remaining (Figure S1).

Assessment of Cell-Penetration of the Protein Dimers. To assess cell penetration via microscopy and flow

https://doi.org/10.1021/acscentsci.1c00663
ACS Cent. Sci. 2021, 7, 1408−1418

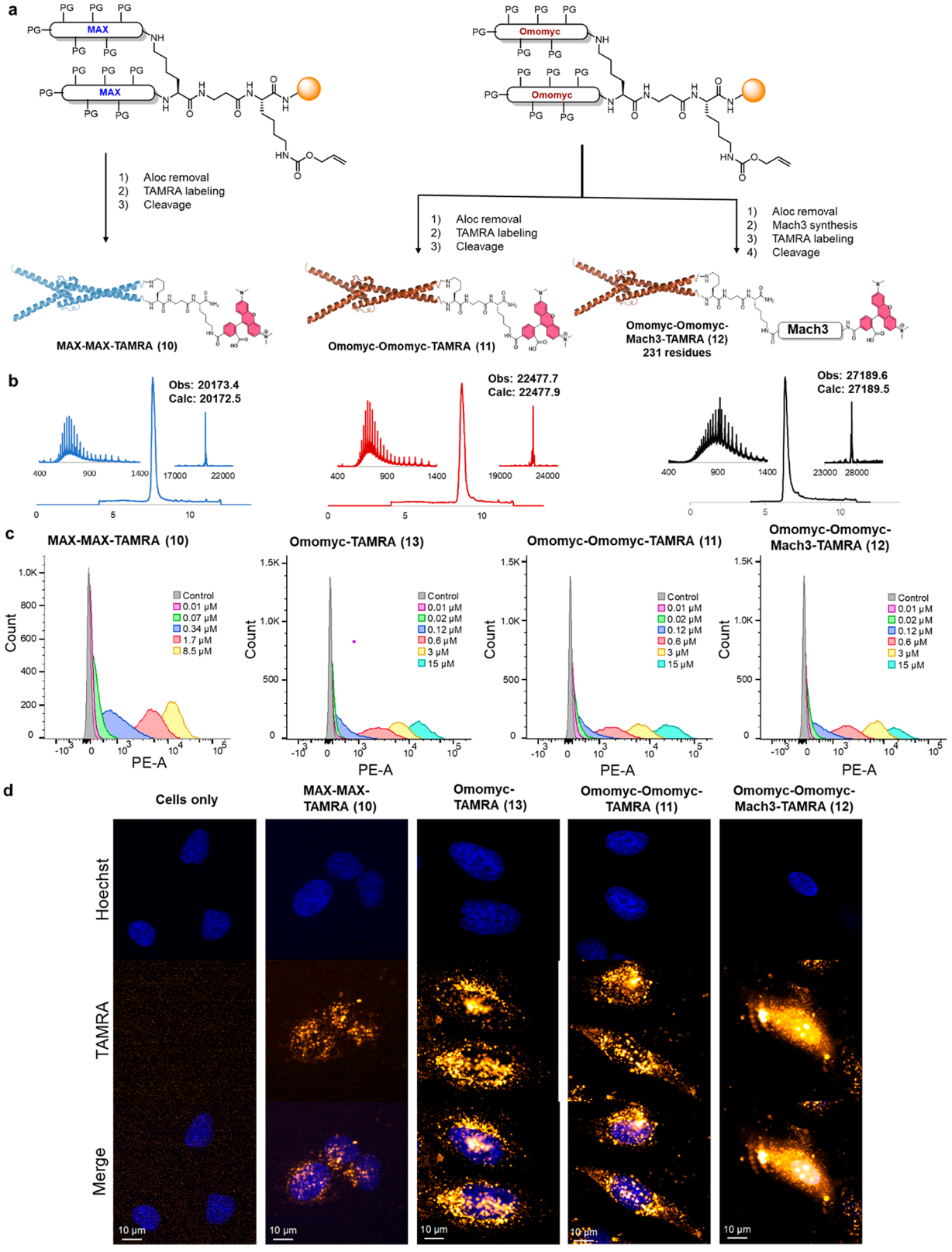

Figure 4. Synthetic dimers are intrinsically cell-penetrating, and nuclear targeting is enhanced by non-natural sequence tags. (a) Reaction conditions. Alloc removal: $Pd(PPh_3)_4$, piperidine, CH_2Cl_2, r.t., 30 min. TAMRA labeling: 5-TAMRA, HATU, DIEA, DMF, r.t., 30 min. Mach3 synthesis: see AFPS conditions (Figure 2c). Cleavage: TFA, EDT, thioanisole, cresol, H_2O, r.t., 4 h. (b) TIC-LCMS chromatograms of MAX−MAX−TAMRA **10**, Omomyc−Omomyc−TAMRA **11**, and Omomyc−Omomyc−Mach3−TAMRA **12** with m/z and deconvoluted mass. (c) Flow cytometry histograms illustrating the dose-dependent increase in fluorescence of HeLa cells after 15 min of incubation with TAMRA-labeled dimers and Omomyc−TAMRA monomer at concentrations between 0.01 and 15 μM. (d) Micrographs from confocal microscopy; Hoechst (DAPI) labels the nuclei, and TAMRA-protein (Cy3) is observed throughout the cell after 15 min of incubation, followed by incubation in fresh media for 1 h.

https://doi.org/10.1021/acscentsci.1c00663
ACS Cent. Sci. 2021, 7, 1408−1418

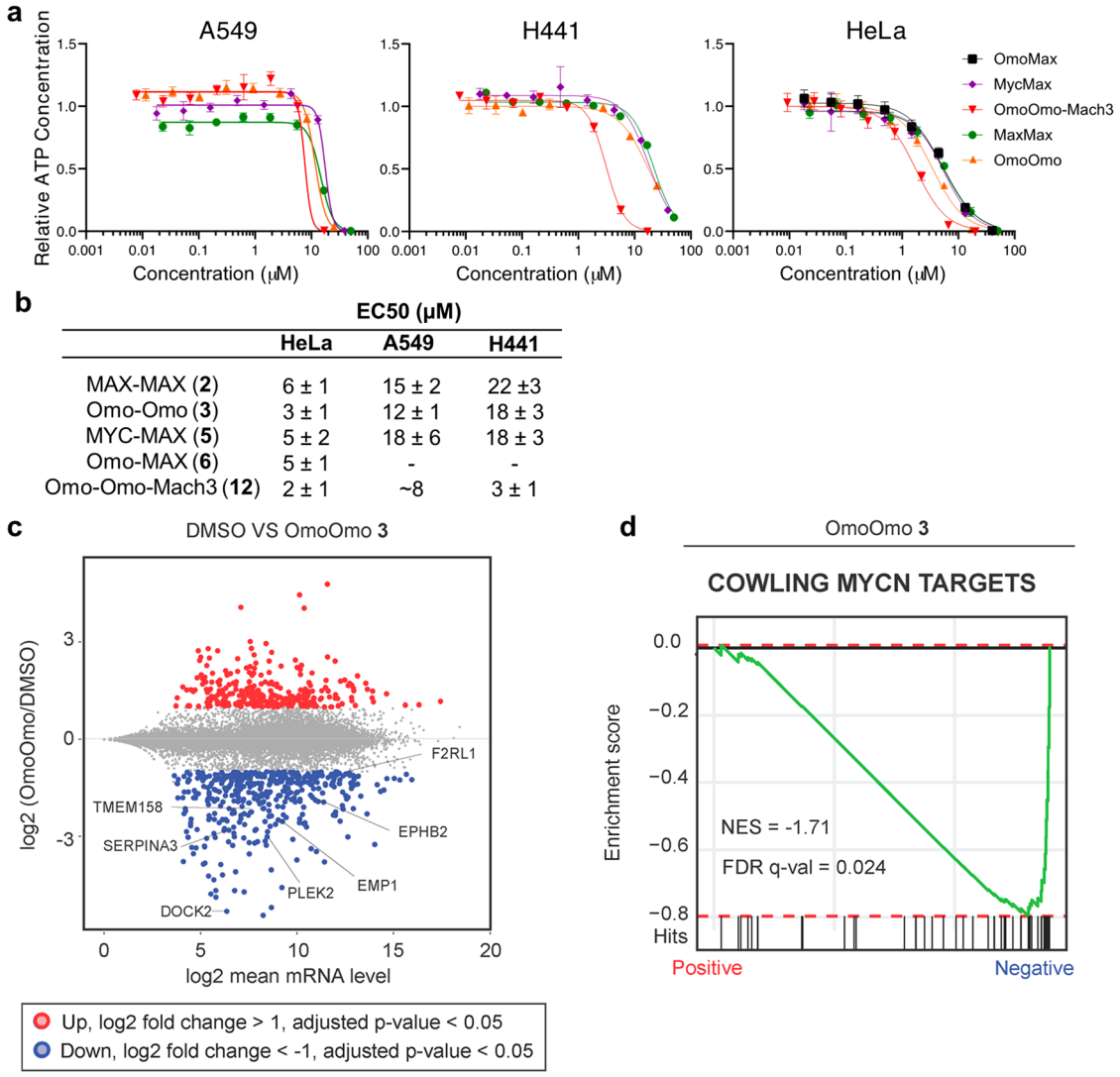

Figure 5. Synthetic transcription factors inhibit cancer cell proliferation and downregulate MYC target genes. (a) Cell proliferation assay of HeLa, A549, and H441 cells following treatment with synthetic protein dimers for 72 h, quantified via CellTiter-Glo (CTG). Experiments were performed in triplicate. (b) Summary table of proliferation inhibition EC_{50} values. (c) A549 cells were treated with Omomyc−Omomyc **3** (12.5 μM) for 72 h. RNA was extracted and sequenced. Depicted is an MA plot showing differentially expressed genes (DEGs) in A549 cells treated with Omomyc−Omomyc **3** compared to DMSO. Upregulated genes with adjusted p-value <0.05 and |log 2FC| ≥ 1 shown in red, downregulated genes with p-value <0.05 and |log 2FC| ≤ 1 shown in blue. The experiment was performed in duplicate. Downregulated genes involved in *KRas* pathways are labeled. (d) GSEA comparing gene expression of DMSO treated cells compared to Omomyc−Omomyc. The enrichment plot of the MYC target gene signature shows a negative enrichment in the Omomyc−Omomyc condition (q-value <0.05).

cytometry, we prepared variants of MAX−MAX and Omomyc−Omomyc labeled with 5-carboxytetramethylrhodamine (TAMRA). We performed the TAMRA labeling on the solid phase, upon Boc protection of the N-termini and removal of the Alloc protection from the C-terminal lysine, obtaining **10** and **11** (Figure 4a). We also synthesized an Omomyc−Omomyc derivative containing Mach3, a nuclear-targeting miniprotein that we recently designed.[45] To obtain this 231 residue covalent protein complex, we removed Alloc from the C-terminal lysine and synthesized, by AFPS, the 41-residue Mach3 sequence from the resulting free amine and finally added a TAMRA label, obtaining compound **12**.

The synthetic dimers are intrinsically cell-penetrating while remaining nonlytic, and nuclear localization is enhanced by the addition of a targeting motif. Omomyc monomer (90 residues) has been shown to be an intrinsically cell-penetrating protein.[26] The arginine-rich DNA binding region appears to be the primary driving force for cell penetration. We recently showed that the combination of multiple cell-penetrating sequences into a single molecule can enhance cell-penetrating activity with a synergistic effect.[46] Based on this rationale, we expected to observe cell-penetrating activity of our dimeric protein complexes containing two polycationic domains. In addition, we were curious if the miniprotein Mach3 could further enhance nuclear localization. To evaluate uptake, we first treated HeLa cells with fluorophore-labeled proteins and measured fluorescence via flow cytometry. All three analogues are taken up into cells in a dose-dependent manner after a brief (15 min) incubation (Figure 4c and Figure S4). The addition of (4′,6-diamidin-2-phenylindol) DAPI as a membrane-impermeable viability dye showed no staining of the gated population of TAMRA-fluorescent cells, suggesting that the constructs entered cells without compromising the membrane (Figures S2 and S3). These findings were confirmed by

https://doi.org/10.1021/acscentsci.1c00663
ACS Cent. Sci. 2021, 7, 1408−1418

fluorescence microscopy. The treatment of HeLa cells for 15 min with MAX−MAX−TAMRA **10** and Omomyc−Omomyc−TAMRA **11** followed by 1 h of incubation in fresh media and imaging via confocal microscopy revealed intense, punctate fluorescence, in agreement with previous observations and our observations on Omomyc (Figure 4d).[26] However, treatment with Omomyc−Omomyc−Mach3 **12** resulted in punctate fluorescence as well as diffuse fluorescence in the nucleus, indicating endosomal escape and nuclear localization (Figure 4d). These experiments show that the dimeric transcription factors are rapidly taken up into cells, and their nuclear localization can be improved with the addition of a non-natural targeting sequence.[47]

Inhibition of Cancer Cell Proliferation and MYC-Driven Transcription upon Omomyc−Omomyc Treatment. The synthetic transcription factor analogue dimers inhibit the proliferation of cancer cells. MYC is known to drive cell proliferation in the majority of human cancers.[14] We reasoned that our synthetic dimers' combined ability to bind E-box DNA and enter cells should result in the inhibition of MYC-dependent gene transcription and cell proliferation. We tested the bioactivity of all compounds in three cell lines with a range of MYC expression levels; HeLa contains high MYC levels, A549 displays mid-level MYC expression, and H441 has low MYC expression.[48] We treated the cells for 72 h with protein dimers and measured the proliferation with a CellTiter-Glo (CTG) assay (Figure 5a). Cell proliferation inhibition followed the expected trend according to MYC expression levels; we observed the most substantial inhibition in HeLa cells and the weakest in H441 cells (Figure 5b). All synthetic dimers demonstrated inhibitory activity, with the Omomyc−Omomyc dimer having the highest activity of the native dimers with an EC_{50} of 4 μM. This observation is in line with our structural stability data. Moreover, Omomyc−Omomyc−Mach3 further decreased the EC_{50} in each cell line (2 μM in HeLa cells), indicating that the nuclear-targeting moiety assists the transcription factor in reaching its target and imparts enhanced activity.

The synthetic transcription factor analogue dimers interfere with MYC-driven gene expression, as determined by RNA-sequencing (RNA-seq) and gene set enrichment analysis (GSEA). To evaluate whether the compounds' bioactivity is related to the suppression of MYC-driven expression, we performed RNA-seq on A549 cells treated with Omomyc−Omomyc **3**. Compared to the control cells, we observed downregulation of 431 and upregulation of 297 genes, indicating that the synthetic dimers have an effect on gene expression (Figure 5c). Among the downregulated genes, we found several genes involved in *KRas* signaling pathways, which are known to drive cancer development in A549 nonsmall lung cancer cells.[46,49] This finding is in accordance with previous reports showing that MYC is a dominant effector of *KRas* mutation-positive lung cancer pathogenesis.[48,50] GSEA of our RNA-seq data shows a negative enrichment of the MYC-target gene set in the Omomyc−Omomyc **3** treated condition, further corroborating that the synthetic dimers interfere with MYC-driven gene expression programs (Figure 5d).

DISCUSSION

We show that flow synthesis enables rapid access to covalently linked homo- and heterodimeric analogues of MYC, MAX, and Omomyc. The automated flow synthesizers developed in our laboratory have been previously shown to provide chemical access to single-domain functional proteins up to 164 residues.[43] Here, we used dimeric linkers and orthogonal protecting group strategies to synthesize homodimeric and heterodimeric proteins with up to 231 residues and synthetic modifications. In our approach, two polypeptide chains are assembled in close proximity to each other, and no significant aggregation events interfered with the efficient double assembly of the dimeric proteins. The use of an orthogonally protected C-terminal lysine residue further enabled the practical late-stage TAMRA labeling of the protein dimers directly on the solid phase.

MYC/MAX is a dimeric transcription factor complex that has been the object of intense studies due to its predominant role in cancer pathogenesis.[9] While the therapeutic targeting of MYC with classical small molecule drugs has been challenging, recent work has indicated that transcription factor analogues themselves, such as Omomyc or MAX, could be used to affect MYC activity.[25,51,52] Omomyc, which inhibits MYC-dependent proliferation in cancer cell lines and mouse models, recently entered human clinical trials.[53]

Given the importance of MYC as a drug target and the challenges related to previous inhibition strategies, our new chemical modalities are of high interest. We showed our dimeric protein complexes being cell-penetrating and interfering with MYC-driven oncogenic transcription. Building on the encouraging data reported for Omomyc, the use of defined covalent protein complexes, as described here, might represent a promising modality for cancer treatment. Indeed, we found our engineered protein dimers having inhibitory activity on MYC-driven proliferation comparable to Omomyc (in the low micromolar range).

Transcription factors might be privileged scaffolds for intracellular delivery. Reaching intracellular targets with biomolecular compounds, such as proteins and oligonucleotides, usually requires the conjugation to cell-penetrating peptides,[54] or the use of delivery vectors.[55] The DNA binding regions of several transcription factors often are polycationic and α-helical, two traits of cell-penetrating peptides.[56] Indeed, several transcription factor proteins were independently shown to be intrinsically cell-penetrating,[57−61] including Soucek's discovery regarding Omomyc.[26] Our group recently reported the synergistic effect of multiple cell-penetrating moieties combined in one sequence.[46] The two cationic helices of the dimeric MYC/MAX mimetics might therefore be the driving force for the intrinsic cell-penetrating activity of these ∼20 kDa macromolecules.

Our parallel protein dimer synthesis mimics nature's strategy of forming protein complexes. Many proteins associate into macromolecular complexes to become functional. Complex formation requires that subunits find each other in the crowded cellular environment while avoiding unspecific interactions. Kramer, Bukau, et al. have recently shown that native protein complex formation is enabled by parallel ribosomal cotranslation, folding, and assembly.[7,8] In close analogy to this biological strategy, we also synthesized our protein dimers in parallel and in close proximity to each other, priming them for correct complex formation.

Dimeric protein complexes, such as bHLH or bZIP (basic leucine zippers), make up hundreds of transcription factors,[62] and our results could define a framework that enables access to several analogues of these families. These synthetic compounds are valuable tools for the study of gene transcription and

https://doi.org/10.1021/acscentsci.1c00663
ACS Cent. Sci. 2021, 7, 1408−1418

possibly disease treatment. We envision that synthetic transcription factor analogues in the future will enable on-demand gene regulation, and our synthesis strategy will enable access to defined protein complexes in their biologically relevant multimeric forms.

METHODS

Manual Preparation of Peptidyl Resins 1 and 4. ChemMatrix Rink Amide resin (loading 0.18 mmol/g, typical scale: 100 mg, 0.02 mmol) was loaded into a fritted syringe (6 mL), swollen in DMF (4 mL) for 5 min, and then drained. Each Nα-Fmoc protected amino acid (0.2 mmol, 10 equiv) was dissolved in DMF containing 0.39 M HATU (0.5 mL). Immediately before the coupling, DIEA (100 μL, 30 equiv) was added to the mixture to activate the amino acid. After 15 s of preactivation, the mixture was added to the resin and reacted for 10 min, with occasional stirring. After completion of the coupling step, the syringe was drained, and the resin was washed with DMF (3 × 5 mL). Fmoc deprotection was performed by the addition of piperidine (20% in DMF, 3 mL) to the resin (1 × 1 min + 1 × 5 min), followed by draining and washing the resin with DMF (5 × 5 mL). For peptidyl resin **1**, the coupling cycles were performed sequentially with Fmoc−Lys(Alloc)−OH, Fmoc−βAla−OH, and Fmoc−Lys(Fmoc)−OH; for peptidyl resin **4**, the coupling cycles were performed sequentially with Fmoc−Lys(Boc)−OH, Fmoc−βAla−OH, and Fmoc−Lys(Alloc)−OH.

Automated Flow Peptide Synthesis (AFPS) Setup. All peptides were synthesized on two automated-flow systems custom built in the Pentelute lab, which are similar to the published AFPS system.[42] The synthesis conditions used are according to Hartrampf et al.:[43] flow-rate = 40 mL/min, temperature = 90 °C (loop 1), 70 °C (loop 2; used for histidine), and 85−90 °C (reactor). The 50 mL/min pump head pumps 400 μL of liquid per pump stroke; the 5 mL/min pump head pumps 40 μL of liquid per pump stroke. The standard synthetic cycle involves a first step of prewashing the resin at elevated temperatures for 60 s at 40 mL/min. During the coupling step, three HPLC pumps are used: a 50 mL/min pump head pumps the activating agent, a second 50 mL/min pump head pumps the amino acid, and a 5 mL/min pump head pumps DIEA. The first two pumps are activated for 8 pumping strokes in order to prime the coupling agent and amino acid before the DIEA pump is activated. The three pumps are then actuated together for a period of 7 pumping strokes, after which the activating agent pump and amino acid pump are switched using a rotary valve to select DMF. The three pumps are actuated together for a final 8 pumping strokes, after which the DIEA pump is shut off, and the other two pumps continue to wash the resin for another 40 pump strokes. During the deprotection step, two HPLC pumps are used. Using a rotary valve, one HPLC pump selects deprotection stock solution and DMF. The pumps are activated for 13 pump strokes. Both solutions are mixed in a 1:1 ratio. Next, the rotary valves select DMF for both HPLC pumps, and the resin is washed for an additional 40 pump strokes. The coupling−deprotection cycle is repeated for all additional monomers.

Manual Boc−Gly−OH coupling. Prior to site-selective modification via the Alloc-protected lysine, we blocked the protein N-termini with Boc−Gly−OH: Peptidyl resin (~10 μmol theoretical loading) was loaded into a fritted syringe (6 mL), swollen in DMF (4 mL) for 5 min, and then drained. Boc−Gly−OH (18 mg, 100 μmol) and HATU (54 mg, 90 μmol) were dissolved in DMF (250 μL), activated with DIEA (38 mg, 52 μL, 300 μmol), added to the peptidyl resin, and incubated for 15 min. After this time, the resin was drained, washed with DMF (3 × 5 mL), and used for the next step.

Alloc Deprotection. The peptidyl resin (~10 μmol theoretical loading) was washed with dichloromethane (3 × 5 mL) and then treated with $Pd(PPh_3)_4$ (11.0 mg, 10 μmol, 1 equiv) in dichloromethane/piperidine (8:2, 1 mL) for 30 min at room temperature under the exclusion of light. The resin was then drained and washed with dichloromethane (3 × 5 mL).

TAMRA Labeling. Peptidyl resin (~10 μmol theoretical loading) was loaded into a fritted syringe (6 mL), swollen in DMF (4 mL) for 5 min, and then drained. 5-Carboxytetramethylrhodamine (5-TAMRA, 22 mg, 50 μmol, 5 equiv) and HATU (17 mg, 45 μmol, 4.5 equiv) were dissolved in DMF (500 μL), activated with DIEA (19 mg, 26 μL, 150 μmol), added to the peptidyl resin, and incubated for 30 min under the exclusion of light. After this time, the resin was drained, washed with DMF (3 × 5 mL), and stored until cleavage.

Cleavage Protocol. After synthesis, the peptidyl resin was washed with dichloromethane (3 × 5 mL) and dried. Approximately 8 mL of cleavage solution (82.5% TFA, 5% water, 5% phenol, 5% thioanisole, 2.5% EDT) was added to the peptidyl resin inside the fritted syringe. The cleavage was kept at room temperature for 4 h, with occasional shaking. After this time, the cleavage mixture was transferred to a falcon tube (through the syringe frit, keeping the resin in the syringe), and the resin was washed with an additional 2 mL of cleavage solution. Ice cold diethyl ether (45 mL) was added to the cleavage mixture, and the precipitate was collected by centrifugation and triturated twice more with cold diethyl ether (45 mL). The supernatant was discarded. Residual ether was allowed to evaporate, and the peptide was dissolved in 50% acetonitrile in water with 0.1% TFA (long peptides were dissolved 70% acetonitrile in water with 0.1% TFA). The peptide solution was filtered with a Nylon 0.22 μm syringe filter, frozen, and then lyophilized until dry.

Polyacrylamide Gel Electrophoresis (PAGE). The analysis was performed using Bolt 4−12% Bis-Tris Plus gels (10 wells) at 165 V for 36 min utilizing prestained Invitrogen SeeBlue Plus2 molecular weight standard. Bolt LDS sample buffer (4×) was added to each protein sample (1 μg) for loading on the gel. The bands were visualized by Coomassie blue staining.

Electrophoretic Mobility Shift Assay (EMSA). The E-Box DNA probe (2 μM in binding buffer) was heated to 95 °C for 5 min and then allowed to cool down to room temperature over 15 min for double-strand annealing. Protein dimer (4 μM in binding buffer: MES 10 mM, KCl 150 mM, $MgCl_2$ 1 mM, TCEP 1 mM, glycerol 10%, pH = 6.5) was added to the DNA (final concentrations: 2 μM protein and 1 μM DNA), and the mixture was incubated for 1 h at room temperature. During the incubation, a 10% polyacrylamide gel was prerun (1 h, 4 °C, 100 V) in 1× TBE buffer. After that time, DNA protein mixture (20 μL) was mixed with 6× DNA loading dye (4 μL)) and loaded on the gel, which was run at 75 V, for 90 min at 4 °C. The gel was washed with water for 20 s and then stained with 0.02% ethidium bromide in 1× TBE buffer for 15 min at room temperature. Bands were visualized on a Biorad Gel imager.

https://doi.org/10.1021/acscentsci.1c00663
ACS Cent. Sci. 2021, 7, 1408−1418

Circular Dichroism (CD). Lyophilized samples were dissolved in folding buffer (MES 10 mM, KCl 150 mM, $MgCl_2$ 1 mM, TCEP 1 mM, glycerol 10%, pH = 6.5) at a final protein concentration of 0.1 mg/mL. The circular dichroism (CD) spectra were obtained using an AVIV 420 circular dichroism spectrometer with a 1 mm path length quartz cuvette. 300 μL samples were used for each measurement. For full wavelength scans, the CD spectra were recorded from 250 to 200 nm at 4 °C with 3 s averaging times at each wavelength. *Y*-axis values are reported in molar ellipticity. For melting temperature determination, CD spectra were recorded at 221 nm from 4 to 89 °C, with +5 °C steps and equilibration times of 60 s at each temperature. For measurements of DNA/protein complexes, equimolar E-Box DNA was added to the proteins in folding buffer; the mixtures were heated to 95 °C for 5 min, allowed to cool down to room temperature over 15 min, and then analyzed.

Cell Culture. HeLa (ATCC CCL-2), A549 (ATCC CCL-185), and H441 (ATCC HTB-174) cancer cell lines were maintained in MEM, FK-12, and RPMI-1640 media each containing 10% v/v fetal bovine serum (FBS) and 1% v/v penicillin–streptomycin, respectively, at 37 °C and 5% CO_2. Cells were passaged at 80% confluency using 0.25% trypsin–EDTA.

Flow Cytometry. HeLa cells were plated at 10 000 cells per well in a 96-well plate the night before the experiment. On the day of the experiment, cells were treated with the indicated concentrations of TAMRA–Omo, TAMRA–OmoOmo, or TAMRA–OmoOmo–Mach3 for 15 min in serum-containing culture medium, washed once with PBS, and treated with 0.25% trypsin–EDTA for 30 min to digest membrane-bound protein, at 37 °C and 5% CO_2. Cells were then washed with PBS, incubated in PBS containing 1× DAPI for 3 min, and then resuspended in PBS containing 2% FBS. Cells were then immediately analyzed on a BD FACS LSR II instrument using DAPI and PE channels.

Cell Proliferation Inhibition Assay. Cells were plated at 5000 cells/well in a 96-well plate the day before the experiment. Synthetic proteins were prepared at varying concentrations in complete media and transferred to the plate. Cells were incubated at 37 °C and 5% CO_2 for 72 h, and cell proliferation was measured using the CellTiter-Glo assay quantified by luminescence.

Microscopy. HeLa cells were plated at 10 000 cells/well in a 96-well 30 mm glass-bottom plate the night before the experiment. On the day of the experiment, cells were treated with TAMRA–Omo, TAMRA–OmoOmo, or TAMRA–OmoOmo–Mach3 (5 μM) in complete medium for 15 min, washed twice with fresh medium, and incubated at 37 °C and 5% CO_2 for 1 h before imaging. Micrographs were obtained on an RPI spinning disk confocal microscope on the RFP setting (561 nm 100 mW OPSL excitation laser, 605/70 nm emission) and DAPI setting (405 nm 100 mW OPSL excitation laser, 450/50 nm emission).

RNA-seq and GSEA. In a 6-well plate, 125 000 A549 cells were plated into each well. The following day, the cells were treated with Omomyc–Omomyc dimer (12.5 μM) in F12K media supplemented with 10% FBS and 1% pen/strep and incubated for 72 h. RNA was isolated using the Qiagen RNeasy Plus mini kit (74136) followed by DNase treatment (AM1906). KAPAHyperRiboErase libraries were prepared and sequenced on a Hi-seq 2500 instrument. Reads from sequencing were aligned using the HISAT2 htseq-count function. Differential gene expression analysis between treated and control cells was performed using the DESEQ2 package in R on raw aligned read counts. The differentially expressed genes were ranked by their log 2FC and adjusted *p*-value. Preranked gene set enrichment analysis (GSEA) was performed using gene sets in the Molecular Signatures Database (MSigBD) to identify MYC-target gene sets.

Safety Statement. No unexpected or unusually high safety hazards were encountered.

■ ASSOCIATED CONTENT

Supporting Information

The Supporting Information is available free of charge at https://pubs.acs.org/doi/10.1021/acscentsci.1c00663.

Synthesis and experimental procedures as well as characterization of all compounds (PDF)

■ AUTHOR INFORMATION

Corresponding Author

Bradley L. Pentelute − *Department of Chemistry and Center for Environmental Health Sciences, Massachusetts Institute of Technology, Cambridge, Massachusetts 02139, United States; The Koch Institute for Integrative Cancer Research, Massachusetts Institute of Technology, Cambridge, Massachusetts 02142, United States; Broad Institute of MIT and Harvard, Cambridge, Massachusetts 02142, United States;* orcid.org/0000-0002-7242-801X; Email: blp@mit.edu

Authors

Sebastian Pomplun − *Department of Chemistry, Massachusetts Institute of Technology, Cambridge, Massachusetts 02139, United States*

Muhammad Jbara − *Department of Chemistry, Massachusetts Institute of Technology, Cambridge, Massachusetts 02139, United States;* orcid.org/0000-0002-4206-5908

Carly K. Schissel − *Department of Chemistry, Massachusetts Institute of Technology, Cambridge, Massachusetts 02139, United States;* orcid.org/0000-0003-0773-5168

Susana Wilson Hawken − *Whitehead Institute for Biomedical Research, Cambridge, Massachusetts 02142, United States; Department of Biology, Massachusetts Institute of Technology, Cambridge, Massachusetts 02139, United States*

Ann Boija − *Whitehead Institute for Biomedical Research, Cambridge, Massachusetts 02142, United States; Department of Biology, Massachusetts Institute of Technology, Cambridge, Massachusetts 02139, United States*

Charles Li − *Whitehead Institute for Biomedical Research, Cambridge, Massachusetts 02142, United States; Department of Biology, Massachusetts Institute of Technology, Cambridge, Massachusetts 02139, United States*

Isaac Klein − *Whitehead Institute for Biomedical Research, Cambridge, Massachusetts 02142, United States; Department of Biology, Massachusetts Institute of Technology, Cambridge, Massachusetts 02139, United States*

Complete contact information is available at: https://pubs.acs.org/10.1021/acscentsci.1c00663

Author Contributions

[▽]S.P. and M.J. contributed equally.

Notes

The authors declare the following competing financial interest(s): B.L.P. is a cofounder of Amide Technologies and Resolute Bio. Both companies focus on the development of protein and peptide therapeutics. MIT is in the process of filing a provisional patent application regarding the compounds described in this study. A.B. is an advisor to Syros Pharmaceuticals.

■ ACKNOWLEDGMENTS

We gratefully acknowledge Prof. Richard A. Young for his generous support of this project. We thank Wendy C. Salmon at the W. M. Keck Microscopy Facility at the Whitehead Institute for help with imaging, and the Swanson Biotechnology Center Flow Cytometry Facility at the Koch Institute for the use of their flow cytometers. C.K.S. (4000057398) acknowledges financial support from the National Science Foundation Graduate Research Fellowship (NSF Grant 1122374). This research was supported by a Bristol-Myers Squibb Unrestricted Grant in Synthetic Organic Chemistry awarded to B.L.P. S.P. thanks the Deutsche Forschungsgemeinschaft for a postdoctoral fellowship (DFG, PO 2413/1-1). M.J. gratefully acknowledges postdoctoral fellowship support from the Rothschild Foundation, the Fulbright Program, and the Israel Council for Higher Education (VATAT). A.B. acknowledges the Swedish Research Council for a postdoctoral fellowship (VR 2017-00372). We thank Dr. Andrei Loas for help with the preparation of this manuscript.

■ REFERENCES

(1) Dawson, P. E.; Muir, T. W.; Clark-Lewis, I.; Kent, S. B. H. Synthesis of Proteins by Native Chemical Ligation. *Science* **1994**, *266*, 776.

(2) Bode, J. W.; Fox, R. M.; Baucom, K. D. Chemoselective Amide Ligations by Decarboxylative Condensations of N-Alkylhydroxylamines and α-Ketoacids. *Angew. Chem., Int. Ed.* **2006**, *45* (8), 1248−1252.

(3) Premdjee, B.; Andersen, A. S.; Larance, M.; Conde-Frieboes, K. W.; Payne, R. J. Chemical Synthesis of Phosphorylated Insulin-like Growth Factor Binding Protein 2. *J. Am. Chem. Soc.* **2021**, *143* (14), 5336−5342.

(4) Agouridas, V.; El Mahdi, O.; Diemer, V.; Cargoët, M.; Monbaliu, J. C. M.; Melnyk, O. Native Chemical Ligation and Extended Methods: Mechanisms, Catalysis, Scope, and Limitations. *Chem. Rev.* **2019**, *119* (12), 7328.

(5) Conibear, A. C.; Watson, E. E.; Payne, R. J.; Becker, C. F. W. Native Chemical Ligation in Protein Synthesis and Semi-Synthesis. *Chem. Soc. Rev.* **2018**, *47* (24), 9046−9068.

(6) Bondalapati, S.; Jbara, M.; Brik, A. Expanding the Chemical Toolbox for the Synthesis of Large and Uniquely Modified Proteins. *Nat. Chem.* **2016**, *8* (5), 407−418.

(7) Bertolini, M.; Fenzl, K.; Kats, I.; Wruck, F.; Tippmann, F.; Schmitt, J.; Auburger, J. J.; Tans, S.; Bukau, B.; Kramer, G. Interactions between Nascent Proteins Translated by Adjacent Ribosomes Drive Homomer Assembly. *Science* **2021**, *371* (6524), 57−64.

(8) Shiber, A.; Döring, K.; Friedrich, U.; Klann, K.; Merker, D.; Zedan, M.; Tippmann, F.; Kramer, G.; Bukau, B. Cotranslational Assembly of Protein Complexes in Eukaryotes Revealed by Ribosome Profiling. *Nature* **2018**, *561* (7722), 268−272.

(9) Meyer, N.; Penn, L. Z. Reflecting on 25 Years with MYC. *Nat. Rev. Cancer* **2008**, *8* (12), 976−990.

(10) Blackwell, T.; Kretzner, L.; Eisenman, R.; Weintraub, H.; Blackwood, E. Sequence-Specific DNA Binding by the c-Myc Protein. *Science* **1990**, *250* (4984), 1149−1151.

(11) Blackwood, E. M.; Eisenman, R. N. Max : A Helix-Loop-Helix Zipper Protein That Complex with Myc. *Science* **1991**, *251*, 1211−1217.

(12) Ferré-D'Amaré, A. R.; Prendergast, G. C.; Ziff, E. B.; Burley, S. K. Recognition by Max of Its Cognate DNA through a Dimeric b/HLH/Z Domain. *Nature* **1993**, *363* (6424), 38−45.

(13) Chen, H.; Liu, H.; Qing, G. Targeting Oncogenic Myc as a Strategy for Cancer Treatment. *Signal Transduct. Target. Ther.* **2018**, *3* (1), 1−7.

(14) Kalkat, M.; De Melo, J.; Hickman, K. A.; Lourenco, C.; Redel, C.; Resetca, D.; Tamachi, A.; Tu, W. B.; Penn, L. Z. MYC Deregulation in Primary Human Cancers. *Genes* **2017**, *8* (6), 151.

(15) Lin, C. Y.; Loven, J.; Rahl, P. B.; Paranal, R. M.; Burge, C. B.; Bradner, J. E.; Lee, T. I.; Young, R. A. Transcriptional Amplification in Tumor Cells with Elevated C-Myc. *Cell* **2012**, *151*, 56−67.

(16) Lee, T. I.; Young, R. A. Transcriptional Regulation and Its Misregulation in Disease. *Cell* **2013**, *152* (6), 1237−1251.

(17) Fletcher, S.; Prochownik, E. V. Small-Molecule Inhibitors of the Myc Oncoprotein. *Biochim. Biophys. Acta, Gene Regul. Mech.* **2015**, *1849* (5), 525−543.

(18) Boike, L.; Cioffi, A. G.; Majewski, F. C.; Co, J.; Henning, N. J.; Jones, M. D.; Liu, G.; McKenna, J. M.; Tallarico, J. A.; Schirle, M.; et al. Discovery of a Functional Covalent Ligand Targeting an Intrinsically Disordered Cysteine within MYC. *Cell Chem. Biol.* **2021**, *28*, 1−10.

(19) Han, H.; Jain, A. D.; Truica, M. I.; Izquierdo-Ferrer, J.; Anker, J. F.; Lysy, B.; Sagar, V.; Luan, Y.; Chalmers, Z. R.; Unno, K.; et al. Small-Molecule MYC Inhibitors Suppress Tumor Growth and Enhance Immunotherapy. *Cancer Cell* **2019**, *36* (5), 483−497.e15.

(20) Koehler, A. N. A Complex Task? Direct Modulation of Transcription Factors with Small Molecules. *Curr. Opin. Chem. Biol.* **2010**, *14* (3), 331−340.

(21) Ulasov, A. V.; Rosenkranz, A. A.; Sobolev, A. S. Transcription Factors: Time to Deliver. *J. Controlled Release* **2018**, *269*, 24−35.

(22) Madden, S. K.; de Araujo, A. D.; Gerhardt, M.; Fairlie, D. P.; Mason, J. M. Taking the Myc out of Cancer: Toward Therapeutic Strategies to Directly Inhibit c-Myc. *Mol. Cancer* **2021**, *20* (1), 1−18.

(23) Struntz, N. B.; Chen, A.; Deutzmann, A.; Wilson, R. M.; Stefan, E.; Evans, H. L.; Ramirez, M. A.; Liang, T.; Caballero, F.; Wildschut, M. H. E.; et al. Stabilization of the Max Homodimer with a Small Molecule Attenuates Myc-Driven Transcription. *Cell Chem. Biol.* **2019**, *26* (5), 711−723.e14.

(24) Soucek, L.; Helmer-Citterich, M.; Sacco, A.; Jucker, R.; Cesareni, G.; Nasi, S. Design and Properties of a Myc Derivative That Efficiently Homodimerizes. *Oncogene* **1998**, *17* (19), 2463−2472.

(25) Massó-Vallés, D.; Soucek, L. Blocking Myc to Treat Cancer: Reflecting on Two Decades of Omomyc. *Cells* **2020**, *9* (4), 883.

(26) Beaulieu, M. E.; Jauset, T.; Massó-Vallés, D.; Martínez-Martín, S.; Rahl, P.; Maltais, L.; Zacarias-Fluck, M. F.; Casacuberta-Serra, S.; Del Pozo, E. S.; Fiore, C.; et al. Intrinsic Cell-Penetrating Activity Propels Omomyc from Proof of Concept to Viable Anti-Myc Therapy. *Sci. Transl. Med.* **2019**, *11* (484), 1−14.

(27) Demma, M. J.; Mapelli, C.; Sun, A.; Bodea, S.; Ruprecht, B.; Javaid, S.; Wiswell, D.; Muise, E.; Chen, S.; Zelina, J.; et al. Omomyc Reveals New Mechanisms To Inhibit the MYC Oncogene. *Mol. Cell. Biol.* **2019**, *39* (22), 1−27.

(28) Lobba, M. J.; Fellmann, C.; Marmelstein, A. M.; Maza, J. C.; Kissman, E. N.; Robinson, S. A.; Staahl, B. T.; Urnes, C.; Lew, R. J.; Mogilevsky, C. S.; et al. Site-Specific Bioconjugation through Enzyme-Catalyzed Tyrosine−Cysteine Bond Formation. *ACS Cent. Sci.* **2020**, *6*, 1564.

(29) Dhanjee, H. H.; Saebi, A.; Buslov, I.; Loftis, A. R.; Buchwald, S. L.; Pentelute, B. L. Protein-Protein Cross-Coupling via Palladium-Protein Oxidative Addition Complexes from Cysteine Residues. *J. Am. Chem. Soc.* **2020**, *142* (20), 9124−9129.

(30) Kumar, K. S. A.; Spasser, L.; Erlich, L. A.; Bavikar, S. N.; Brik, A. Total Chemical Synthesis of Di-Ubiquitin Chains. *Angew. Chem., Int. Ed.* **2010**, *49* (48), 9126−9131.

https://doi.org/10.1021/acscentsci.1c00663
ACS Cent. Sci. 2021, 7, 1408−1418

(31) Chatterjee, C.; McGinty, R. K.; Pellois, J.-P.; Muir, T. W. Auxiliary-Mediated Site-Specific Peptide Ubiquitylation. *Angew. Chem., Int. Ed.* **2007**, *119* (16), 2872−2876.
(32) Ajish Kumar, K. S.; Haj-Yahya, M.; Olschewski, D.; Lashuel, H. A.; Brik, A. Highly Efficient and Chemoselective Peptide Ubiquitylation. *Angew. Chem., Int. Ed.* **2009**, *48* (43), 8090−8094.
(33) Fottner, M.; Brunner, A. D.; Bittl, V.; Horn-Ghetko, D.; Jussupow, A.; Kaila, V. R. I.; Bremm, A.; Lang, K. Site-Specific Ubiquitylation and SUMOylation Using Genetic-Code Expansion and Sortase. *Nat. Chem. Biol.* **2019**, *15* (3), 276−284.
(34) Sui, X.; Wang, Y.; Du, Y. X.; Liang, L. J.; Zheng, Q.; Li, Y. M.; Liu, L. Development and Application of Ubiquitin-Based Chemical Probes. *Chem. Sci.* **2020**, *11* (47), 12633−12646.
(35) Geurink, P. P.; El Oualid, F.; Jonker, A.; Hameed, D. S.; Ovaa, H. A General Chemical Ligation Approach Towards Isopeptide-Linked Ubiquitin and Ubiquitin-Like Assay Reagents. *ChemBioChem* **2012**, *13* (2), 293−297.
(36) Kulkarni, S. S.; Sayers, J.; Premdjee, B.; Payne, R. J. Rapid and Efficient Protein Synthesis through Expansion of the Native Chemical Ligation Concept. *Nat. Rev. Chem.* **2018**, *2* (4), 1−17.
(37) Pan, M.; Gao, S.; Zheng, Y.; Tan, X.; Lan, H.; Tan, X.; Sun, D.; Lu, L.; Wang, T.; Zheng, Q.; et al. Quasi-Racemic X-Ray Structures of K27-Linked Ubiquitin Chains Prepared by Total Chemical Synthesis. *J. Am. Chem. Soc.* **2016**, *138* (23), 7429−7435.
(38) Jbara, M.; Laps, S.; Morgan, M.; Kamnesky, G.; Mann, G.; Wolberger, C.; Brik, A. Palladium Prompted On-Demand Cysteine Chemistry for the Synthesis of Challenging and Uniquely Modified Proteins. *Nat. Commun.* **2018**, *9* (1), 3154.
(39) Torbeev, V. Y.; Raghuraman, H.; Hamelberg, D.; Tonelli, M.; Westler, W. M.; Perozo, E.; Kent, S. B. H. Protein Conformational Dynamics in the Mechanism of HIV-1 Protease Catalysis. *Proc. Natl. Acad. Sci. U. S. A.* **2011**, *108* (52), 20982−20987.
(40) Nair, S. K.; Burley, S. K. X-Ray Structures of Myc-Max and Mad-Max Recognizing DNA: Molecular Bases of Regulation by Proto-Oncogenic Transcription Factors. *Cell* **2003**, *112* (2), 193−205.
(41) Canne, L. E.; Ferré-D'Amaré, A. R.; Burley, S. K.; Kent, S. B. H. Total Chemical Synthesis of a Unique Transcription Factor-Related Protein: CMyc—Max. *J. Am. Chem. Soc.* **1995**, *117* (11), 2998−3007.
(42) Mijalis, A. J.; Thomas, D. A.; Simon, M. D.; Adamo, A.; Beaumont, R.; Jensen, K. F.; Pentelute, B. L. A Fully Automated Flow-Based Approach for Accelerated Peptide Synthesis. *Nat. Chem. Biol.* **2017**, *13* (5), 464−466.
(43) Hartrampf, N.; Saebi, A.; Poskus, M.; Gates, Z. P.; Callahan, A. J.; Cowfer, A. E.; Hanna, S.; Antilla, S.; Schissel, C. K.; Quartararo, A. J.; et al. Synthesis of Proteins by Automated Flow Chemistry. *Science* **2020**, *368* (6494), 980−987.
(44) Palmacci, E. R.; Plante, O. J.; Hewitt, M. C.; Seeberger, P. H. Automated Synthesis of Oligosaccharides. *Helv. Chim. Acta* **2003**, *86*, 3975.
(45) Schissel, C.; Mohapatra, S.; Wolfe, J.; Fadzen, C.; Bellovoda, K.; Wu, C.-L.; Wood, J.; Malmberg, A.; Loas, A.; Gómez-Bombarelli, R.; et al. Interpretable Deep Learning for De Novo Design of Cell-Penetrating Abiotic Polymers. bioRxiv, 2020. https://doi.org/10.1101/2020.04.10.036566.
(46) Fadzen, C. M.; Holden, R. L.; Wolfe, J. M.; Choo, Z. N.; Schissel, C. K.; Yao, M.; Hanson, G. J.; Pentelute, B. L. Chimeras of Cell-Penetrating Peptides Demonstrate Synergistic Improvement in Antisense Efficacy. *Biochemistry* **2019**, *58* (38), 3980−3989.
(47) Wang, E.; Sorolla, A.; Cunningham, P. T.; Bogdawa, H. M.; Beck, S.; Golden, E.; Dewhurst, R. E.; Florez, L.; Cruickshank, M. N.; Hoffmann, K.; et al. Tumor Penetrating Peptides Inhibiting MYC as a Potent Targeted Therapeutic Strategy for Triple-Negative Breast Cancers. *Oncogene* **2019**, *38* (1), 140−150.
(48) Fukazawa, T.; Maeda, Y.; Matsuoka, J.; Yamatsuji, T.; Shigemitsu, K.; Morita, I.; Faiola, F.; Durbin, M. L.; Soucek, L.; Naomoto, Y. Inhibition of Myc Effectively Targets KRAS Mutation-Positive Lung Cancer Expressing High Levels of Myc. *Anticancer Res.* **2010**, *30* (10), 4193−4200.
(49) Spiegel, J.; Cromm, P. M.; Zimmermann, G.; Grossmann, T. N.; Waldmann, H. Small-Molecule Modulation of Ras Signaling. *Nat. Chem. Biol.* **2014**, *10* (8), 613−622.
(50) Johnson, C. D.; Esquela-Kerscher, A.; Stefani, G.; Byrom, M.; Kelnar, K.; Ovcharenko, D.; Wilson, M.; Wang, X.; Shelton, J.; Shingara, J.; et al. The Let-7 MicroRNA Represses Cell Proliferation Pathways in Human Cells. *Cancer Res.* **2007**, *67* (16), 7713−7722.
(51) Jung, L. A.; Gebhardt, A.; Koelmel, W.; Ade, C. P.; Walz, S.; Kuper, J.; Von Eyss, B.; Letschert, S.; Redel, C.; D'Artista, L.; et al. OmoMYC Blunts Promoter Invasion by Oncogenic MYC to Inhibit Gene Expression Characteristic of MYC-Dependent Tumors. *Oncogene* **2017**, *36* (14), 1911−1924.
(52) Montagne, M.; Beaudoin, N.; Fortin, D.; Lavoie, C. L.; Klinck, R.; Lavigne, P. The Max B-HLH-LZ Can Transduce into Cells and Inhibit c-Myc Transcriptional Activities. *PLoS One* **2012**, *7* (2), 2−10.
(53) *Peptomyc*. https://www.biospace.com/article/releases/peptomyc-s-omomyc-based-therapy-omo-103-has-obtained-approval-for-first-in-human-phase-i-ii-trial-to-assess-the-efficacy-and-safety-of-a-novel-myc-inhibitor/.
(54) Herce, H. D.; Schumacher, D.; Schneider, A. F. L.; Ludwig, A. K.; Mann, F. A.; Fillies, M.; Kasper, M. A.; Reinke, S.; Krause, E.; Leonhardt, H.; et al. Cell-Permeable Nanobodies for Targeted Immunolabelling and Antigen Manipulation in Living Cells. *Nat. Chem.* **2017**, *9* (8), 762−771.
(55) Gersbach, C. A.; Gaj, T.; Barbas, C. F. Synthetic Zinc Finger Proteins: The Advent of Targeted Gene Regulation and Genome Modification Technologies. *Acc. Chem. Res.* **2014**, *47* (8), 2309−2318.
(56) Eiríksdóttir, E.; Konate, K.; Langel, Ü.; Divita, G.; Deshayes, S. Secondary Structure of Cell-Penetrating Peptides Controls Membrane Interaction and Insertion. *Biochim. Biophys. Acta, Biomembr.* **2010**, *1798* (6), 1119−1128.
(57) Gaj, T.; Guo, J.; Kato, Y.; Sirk, S. J.; Barbas, C. F. Targeted Gene Knockout by Direct Delivery of Zinc-Finger Nuclease Proteins. *Nat. Methods* **2012**, *9* (8), 805−807.
(58) Gaj, T.; Liu, J.; Anderson, K. E.; Sirk, S. J.; Barbas, C. F. Protein Delivery Using Cys2-His2 Zinc-Finger Domains. *ACS Chem. Biol.* **2014**, *9* (8), 1662−1667.
(59) Knox, S. L.; Wissner, R.; Piszkiewicz, S.; Schepartz, A. Cytosolic Delivery of Argininosuccinate Synthetase Using a Cell- Permeant Miniature Protein. *ACS Cent. Sci.* **2021**, *7*, 641−649.
(60) Libetti, D.; Bernardini, A.; Chiaramonte, M. L.; Minuzzo, M.; Gnesutta, N.; Messina, G.; Dolfini, D.; Mantovani, R. NF-YA Enters Cells through Cell Penetrating Peptides. *Biochim. Biophys. Acta, Mol. Cell Res.* **2019**, *1866* (3), 430−440.
(61) Zhang, Z.; Bu, H.; Yu, J.; Chen, Y.; Pei, C.; Yu, L.; Huang, X.; Tan, G.; Tan, Y. The Cell-Penetrating FOXM1 N-Terminus (M1−138) Demonstrates Potent Inhibitory Effects on Cancer Cells by Targeting FOXM1 and FOXM1-Interacting Factor SMAD3. *Theranostics* **2019**, *9* (10), 2882−2896.
(62) Lambert, S. A.; Jolma, A.; Campitelli, L. F.; Das, P. K.; Yin, Y.; Albu, M.; Chen, X.; Taipale, J.; Hughes, T. R.; Weirauch, M. T. The Human Transcription Factors. *Cell* **2018**, *172* (4), 650−665.